

When there is a discrepancy between the information in this technical report and information in JDox, assume JDox is correct.



JWST TECHNICAL REPORT

Title: OTE Science Performance Memo 7: The Optimal Wavefront Control Threshold	Doc #: JWST-STScI-009318 Date: 15 April 2026 Rev: -
Authors: Roeland P. van der Marel	Release Date: 27 April 2026

Table of Contents

ABSTRACT.....	2
1 Introduction.....	3
2 Analytical Treatment	4
2.1 Encircled Energy Evolution.....	4
2.2 Signal-to-Noise Ratio Evolution.....	5
2.3 Wavefront Control Strategy	6
3 Relation between Encircled Energy and Wavefront Error	8
4 Time breakdown of JWST Usage.....	10
4.1 On-sky Science Time Fraction.....	10
4.2 Observing Mode Dependence.....	12
4.3 Combined Results	15
5 Interpretation and Conclusions	16
6 Acknowledgements.....	18
7 Bibliography	19

Operated by the Association of Universities for Research in Astronomy, Inc., for the National Aeronautics and Space Administration under Contract NAS5-03127

OTE Science Performance Memo VII: The Optimal Wavefront Control Threshold

Roeland P. van der Marel

Space Telescope Science Institute, Baltimore, MD

April 15, 2026

ABSTRACT

The segmented JWST primary mirror is kept in alignment by a process of Wavefront Sensing and Control (WFS&C), based on NIRCcam sensing observations of defocused bright stars. A mirror control activity is executed every time the sensed wavefront error (WFE) has increased by ΔWFE since the last control. We derive the optimal value of ΔWFE so as to minimize the total amount of time required for a given sequence of science observations, with any interspersed control activities, to attain a fixed signal-to-noise ratio (S/N). The result depends on the fractional decrease in encircled energy as function of WFE, which is more significant at smaller wavelengths; and on the efficiency and composition of the overall JWST observing program. We analyze the former using simulated point spread functions with STPSF, and the latter using a detailed breakdown of the accepted pool of JWST programs. While the current operational threshold is $\Delta WFE = 8$ nm (implying an average control cadence of ~ 3.05 months, given observed WFE drift rates), we derive instead an optimal $\Delta WFE = 1.80 \pm 0.45$ nm (yielding an average control cadence of 23.4 ± 7.5 days). If ΔWFE were lowered accordingly, and concurrently the sensing cadence were increased from 4 days to 4.5 days, there would be no change in total operational WFS&C overheads. An increased WFS cadence would itself provide a more efficient use of observatory time, per the arguments previously presented in van der Marel (2025). Hence, increasing the WFC cadence, while slightly decreasing the WFS cadence, would (very slightly) improve the aggregate S/N and efficiency of the JWST science program. However, any new criterion that affects these cadences should also take into account additional operational considerations.

1 Introduction

The James Webb Space Telescope (JWST; e.g., Gardner et al. 2023) has a lightweight segmented primary mirror composed of 18 distinct segments attached to a common backplane structure. During the commissioning of the Optical Telescope Element (OTE), the telescope was brought into focus using an extensive multi-step alignment process (McElwain et al. 2023). Following this, periodic adjustments using 126 distinct actuators remain necessary to keep the telescope in alignment. This is accomplished using a process of Wavefront Sensing and Control (WFS&C). NIRCам Wave Front Sensing (WFS) observations of defocused bright stars are taken on a regular cadence. These observations are processed and analyzed at STScI using software developed pre-launch by Ball Aerospace. A Wave Front Control (WFC) activity can then be executed some days later whenever deemed necessary.

Prior to launch, integrated modeling of thermal drifts suggested that WFC may be necessary every 2 weeks to continue to meet image quality requirements. However, the OTE alignment achieved after commissioning was significantly below requirements, and better than had been foreseen. Since then, the RMS wavefront error (WFE) has evolved through a combination of slow linear increases interspersed with discontinuous jumps (e.g., Lajoie et al. 2023; van der Marel et al. 2025, hereafter OTE Memo #5). Yet, the WFE has exceeded requirements only twice during the years since the start of science operations. This raised the question what would be a more appropriate trigger for executing WFC activities. In response, a flexible set of criteria was adopted with both community science and operational considerations in mind (Flagey et al. 2025). The most important criterion was that a WFC would be executed whenever the WFE exceeds a threshold of $\Delta WFE = 8$ nm above the state achieved after the previous WFC. This remains one of the operational thresholds for WFC at the time of this writing (see Figure 1 of OTE Memo #5).

A threshold value of 8 nm is somewhat arbitrary. Initially after commissioning, while the observatory was still settling down, this yielded WFC activities on roughly the 2-week cadence foreseen before launch. But as the telescope has become more stable over time, WFC activities are now few and far between. In absence of occasional discontinuous jumps (now ~ 5 per year), it currently takes the observatory WFE on average ~ 3 months to increase by 8 nm (OTE Memo #5). This implies that the observatory is operated for long times with slowly deteriorating image quality. This suggests that maybe the threshold should be lowered. However, this prompts the question: what is the "optimal" threshold?

One metric that can shed light on this issue is that of optimal use of observing time. Consider a hypothetical set of JWST observing programs that all need to achieve a prescribed signal-to-noise ratio (S/N). At a lower image quality, it takes longer to reach the given S/N . Thus, if a WFC is executed too rarely, this wastes observing time. Yet if a WFC is executed too frequently, this takes too much time away from science observations (a WFC requires an added ~ 47 minutes, during which no science observations can be done). Between these extremes, there is an optimum WFC cadence that minimizes the amount of wall clock time required to execute all observations to specification. Given the average slope at which WFE increases with time, this

cadence corresponds to a particular Δ WFE threshold. The present report calculates this threshold and discusses its implications for JWST operations.

The outline of this report is as follows. In Section 2 we present an analytical framework to derive an equation for the optimal Δ WFE threshold. Table 1 summarizes, for ease of reference, those quantities introduced that are used throughout this report. In Section 3 we analyze simulated JWST point-spread functions (PSFs), to determine how the encircled energy at various wavelengths depends on WFE. This is a key quantity in the equation for Δ WFE. In Section 4 we discuss how, broadly speaking, JWST observing time is used for different types of observations and activities. This is relevant since S/N considerations differ for different observing modes and target types. We then use this to estimate how the S/N of the overall JWST observing program is affected by variations in WFE, and from this we determine the optimal WFE threshold. In Section 5 we interpret and discuss the results and make operational recommendations for further consideration.

2 Analytical Treatment

2.1 Encircled Energy Evolution

Operational experience with the JWST OTE (e.g., Figure 1 of OTE Memo #5) has shown that, in the absence of occasional discrete jumps, the WFE drifts linearly with time

$$\text{WFE} = \text{WFE}_0 + s_w t' \quad . \quad (1)$$

Here s_w is the slope of the increase, WFE_0 is the WFE achieved after a WFC activity, and t' is the time elapsed since that activity.

The encircled energy inside a fixed aperture of radius R that is associated with a given WFE can be expanded in a first-order Taylor series as

$$\text{EE} = \text{EE}_0 [1 - s_e (\text{WFE} - \text{WFE}_0)] \quad . \quad (2)$$

Here EE_0 is the encircled energy achieved after a WFC activity, and s_e quantifies the fractional decrease in EE with increasing WFE. The dependence of EE on WFE is further quantified in Section 3, yielding estimates of s_e , and demonstrating that the linear approximation is reasonable over the small changes $\text{WFE} - \text{WFE}_0$ of interest here.

Substitution of equation (2) in equation (1) yields

$$\text{EE} = \text{EE}_0 [1 - s_e s_w t'] \quad , \quad (3)$$

so that the encircled energy decreases approximately linearly with time after a WFC.

Table 1: Summary Listing of Model Quantities and Parameters

Quantity/ Parameter	Nominal Value	Definition
<i>JWST Observing Program</i>		
η	0.604 ± 0.05^1	Fraction of the time JWST collects photons from on-sky science exposures
$\zeta_{...}$		Fraction of the time used for a particular mode or type of observations (as indicated by the subscript)
f_{app}	0.50 ± 0.25^2	Fraction of targets to which S/N considerations of Section 2.2 apply (faint background-limited point sources)
ξ	0.223 ± 0.063^3	Fraction of the total time to which S/N considerations of Section 2.2 apply
T_{max}		Time interval during which observations are executed
<i>Telescope Behavior</i>		
WFE		RMS OTE Wavefront Error
WFE_0		WFE after a WFC
s_w	0.0862 nm/day^4	Linear slope with which RMS OTE WFE drifts upward after a WFC
t'		Time since last WFC
<i>Wavefront Sensing and Control Operations</i>		
D_s	51 min^4	Duration of a wavefront sensing observation
D_c	98 min^4	Duration of a WFC activity
ΔT_c	47 min	Extra time required for a WFC activity ($= D_c - D_s$)
ΔWFE	$1.80 \pm 0.45 \text{ nm}^5$	Increase in RMS OTE WFE over the baseline to trigger a wavefront control (as implied by present formalism; current operational value is 8nm)
ΔT_{WFC}	$23.4 \pm 7.5 \text{ days}^6$	average cadence between WFC activities (i.e., $\Delta \text{WFE}/s_w$)
$\Delta \text{IW}_{\text{opt}}$	$20.5 \pm 9.2 \text{ nm day}^7$	integrated WFE increase ΔIW relative to the baseline to trigger a WFC
<i>Point Spread Function</i>		
FWHM	Table 2	Full Width at Half Maximum of the PSF
R_{opt}	Eq. (17)	Aperture radius that yields the optimal S/N
EE		Encircled Energy inside an aperture of radius R (usually R_{opt})
EE_0	Table 2	EE after a WFC
s_e	Table 2	Slope of fractional decrease of EE/EE_0 as function of WFE
$\langle s_e \rangle_{...}$	Eqs. (18-20),(22)	Average value of s_e over different filters or observing modes (as indicated by the subscript)
<i>Observations</i>		
S/N		Signal-to-Noise ratio of an observation
T_0		Canonical exposure time at $t' = 0$ that yields a given S/N
T'		Exposure time at a different time t' that yields the same S/N
<i>Analytical Treatment</i>		
β		Auxiliary quantity defined in eq. (9)

2.2 Signal-to-Noise Ratio Evolution

We now consider the impact of a change in encircled energy on the S/N of a faint point source in imaging mode and in the background limited regime (i.e., unlike for bright sources, the noise is dominated by the noise from the background and not the noise from the point source itself). Let

¹ Section 4.1

² Section 4.2.3

³ equation (21)

⁴ OTE Memo #5

⁵ equation (23)

⁶ equation (24)

⁷ equation (26)

the point source have a brightness that yields p photons/s on the detector; and let the background contribute b photons/s/arcsec² on the detector. The S/N in a total on-sky integration of time T_0 , obtained right after a WFC, is then

$$[S/N] = EE_0 p T_0 / \sqrt{(\pi R^2 b T_0)} \quad . \quad (4)$$

At a later time characterized by encircled energy EE , and with a possibly different exposure time T' , the S/N will be

$$[S/N]' = EE p T' / \sqrt{(\pi R^2 b T')} \quad . \quad (5)$$

If we choose the exposure time T' so that S/N remains the same, then

$$(T'/T_0) = (EE/EE_0)^{-2} \quad . \quad (6)$$

Substitution of equation (3) yields that

$$(T'/T_0) = (1 - [s_e s_w t'])^{-2} \quad . \quad (7)$$

In the regime of small variations in encircled energy this can be approximated using a first-order Taylor expansion as

$$(T'/T_0) = 1 + \beta t' \quad . \quad (8)$$

where we have defined

$$\beta = 2 s_e s_w \quad . \quad (9)$$

2.3 Wavefront Control Strategy

The *average* exposure time for a series of exposures that all reach the same S/N , and which are evenly spread in time between $t' = 0$ and $t' = T_{\max}$ scales as

$$(1/T_{\max}) \int_0^{T_{\max}} (T'/T_0) dt' = 1 + (\beta T_{\max}/2) \quad , \quad (10)$$

which was evaluated by integrating equation (8). If there is no degradation in WFE then $s_w = 0$, so that $\beta = 0$, and equation (10) reduces to unity.

In any period of wall clock length T_{\max} , JWST will only be spending a fraction ξ of its time performing on-sky integrations of the kind that are well described by the aforementioned equations. This implies that the total *extra* exposure time that needs to be spent to obtain exposures of the same S/N , compared to the no WFE-evolution case, equals

$$\Delta T^- = \xi \beta T_{\max}^2 / 2 \quad . \quad (11)$$

This corresponds to the scenario in which no WFC is performed (as indicated by a minus sign) over the period T_{\max} . However, we could alternatively perform a WFC (indicated by a plus sign) at some time $t' = \alpha T_{\max}$, where $\alpha \in [0,1]$. The total extra exposure time is then instead

$$\Delta T^+ = (\xi \beta T_{\max}^2 / 2) (\alpha^2 + [1 - \alpha]^2) \quad . \quad (12)$$

The second factor in parentheses has a minimum value 1/2 that is attained at $\alpha = 1/2$. Hence, the WFC is best done mid-way through the period of length T_{\max} , for which

$$\Delta T_{\text{mid}}^+ = \Delta T^- / 2 \quad . \quad (13)$$

Hence, this strategy provides a savings in exposure time relative to the no-WFC scenario equal to $\Delta T^- - \Delta T_{\text{mid}}^+ = \Delta T^- / 2$.

Performing a WFC does require an extra investment of time $\Delta T_c = D_c - D_s$, being the extra time required for a WFC visit (of duration D_c , which consists of a sensing, a control, and another sensing) instead of a regular recurring WFS visit (of duration D_s). Hence, performing a WFC only provides a net savings if $\Delta T^- / 2 > \Delta T_c$. Substitution of equation (11) yields that the break-even point is at

$$T_{\text{max-be}} = \sqrt{(4 \Delta T_c / \xi \beta)} \quad . \quad (14)$$

A WFC would have to be done midway through this period, so per equation (1) the $\Delta \text{WFE} = \text{WFE} - \text{WFE}_0$ that has accumulated over that time equals $s_w (T_{\text{max-be}} / 2)$. Substitution of equations (9) and (14) then yields

$$\Delta \text{WFE} = \sqrt{(\Delta T_c s_w / 2 \xi s_e)} \quad . \quad (15)$$

Once the increase in WFE has reached this threshold, it is better to perform a WFC rather than continue to observe with further deteriorating image quality. At this threshold, the average cadence between WFC activities equals $\Delta \text{WFE} / s_w$.

When there are observation sequences in multiple filters i , which each have their own value s_{ei} , equation (15) still holds. In this case the weighted average value

$$\langle s_e \rangle = \sum_i f_{\text{usage},i} s_{ei} \quad (16)$$

should be used, where $f_{\text{usage},i}$ are the fractions (summing to 1) of the observing time in each of the filters.

3 Relation between Encircled Energy and Wavefront Error

To derive relations between EE and WFE, as required for equation (2), we used data from the period from March 31 to Oct 3, 2024. During this time the WFE drifted slowly and near-linearly for about half a year, without interruption from discontinuous jumps (see e.g. Figure 1 and Table 4 in OTE Memo #5). For each WFS observation performed during this period, we used STPSF to retrieve the inferred Optical Path Difference (OPD) map over the pupil. From this we determined the PSF, EE curve and FWHM for all of the wide-band filters of the Near Infrared Camera (NIRCam).

To measure an encircled energy, one must choose an aperture size. If the aperture is small, only little light from the source is included. However, if the aperture is increased too much, mostly noise from the background gets added without significantly increasing the source signal. Hence, the S/N is low for both small and larger apertures, and there is an intermediate "optimal" aperture size R_{opt} at which the S/N is maximized. Savino et al. (2024) quantified this aperture size and showed that it scales near-linearly with the PSF FWHM. A polynomial fit to their Figure 5 and Table 2 yields

$$R_{\text{opt}} = (0.7578 \text{ FWHM}) + 0.0008 - (1.2505 \text{ FWHM}^2) \quad , \quad (17)$$

with all quantities in arcsec. The first term in this equation dominates, while the second and third terms provide small corrections. For each filter we used this relation to determine the optimal aperture size for the PSF on April 21, 2024, which had the lowest RMS WFE over this period.⁸ For this date, we denote the FWHM as FWHM_0 , the optimal aperture size as $R_{\text{opt}0}$, and the encircled energy within this aperture, as EE_0 . We then used this same aperture size to determine the encircled energy for all the other dates.

Figure 1 shows the results for EE/EE_0 versus WFE for all eight of the NIRCam wide-band filters⁹. Linear fits to the data are shown as solid lines; the slopes of these lines correspond to s_e , according to equation (2). These fits reproduce the data well. Table 2 reports for each filter the values of FWHM_0 , $R_{\text{opt}0}$, EE_0 , and s_e . The slopes s_e decrease with increasing wavelength. This is as expected, given that a fixed WFE is a lower fraction at larger wavelengths, thus having less impact on the PSF.

⁸ Interestingly, this was 3 weeks after a WFC was performed, due to a temporary spontaneous OTE reversion to a slightly better aligned state.

⁹ The jupyter notebook that was created to generate Figure 1 and the data in Table 2 is available at https://github.com/rpvdmarel/WFC_threshold

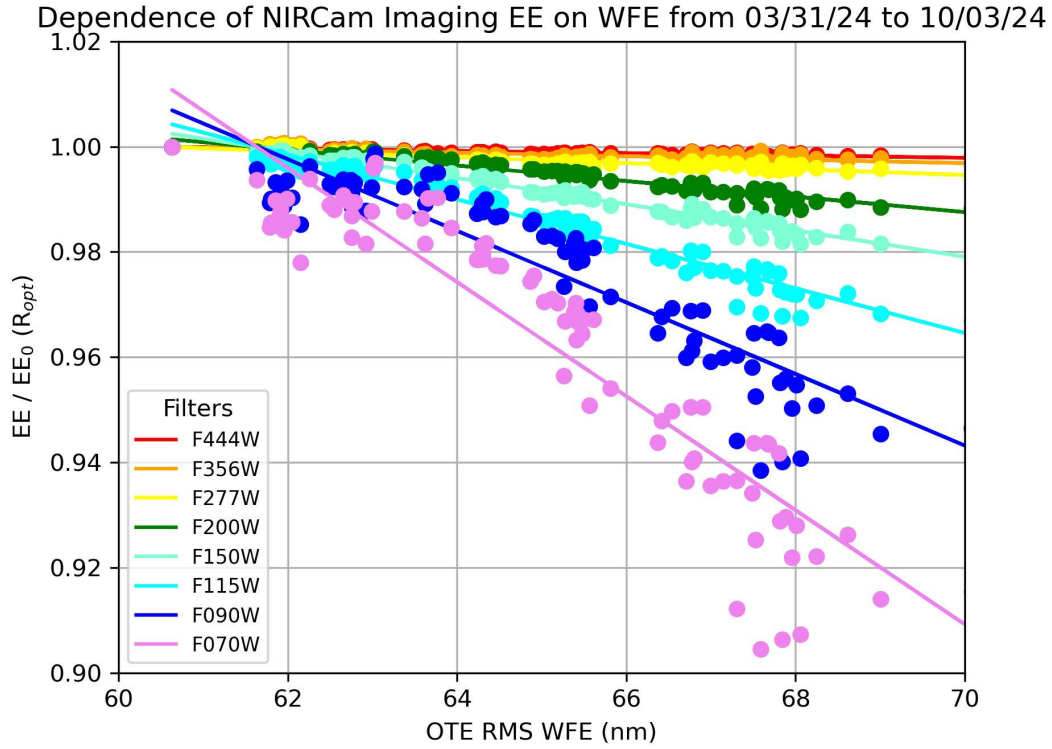


Figure 1. Fractional decrease in EE inside the optimal aperture radius R_{opt} vs. OTE RMS WFE. Based on simulated PSFs for the wide-band NIRCcam filters using operational OPD maps inferred from WFS between March 31 and Oct 3, 2024. Straight-line fits are shown, which have the slope value s_e listed in Table 2.

Table 2: Simulated NIRCcam Wide-Filter PSF Characteristics

Filter	FWHM (arcsec)	R_{opt} (arcsec)	EE_0	s_e (10^{-3} nm^{-1})	f_{usage}
F070W	0.023	0.017	0.42	10.84	0.03
F090W	0.029	0.022	0.50	6.80	0.06
F115W	0.037	0.027	0.55	4.23	0.13
F150W	0.048	0.035	0.54	2.49	0.14
F200W	0.064	0.044	0.53	1.48	0.14
F277W	0.088	0.058	0.53	0.565	0.16
F356W	0.114	0.071	0.49	0.330	0.14
F444W	0.140	0.083	0.46	0.224	0.20

Notes: *Column #1:* Filter name; light-gray rows correspond to the SW channel and dark gray lines to the LW channel. *Column #2:* FWHM for the PSF on April 21, 2024. *Column #3:* Optimal aperture radius based equation (17), derived from Savino et al. (2024). *Column #4:* Encircled energy within this radius. *Column #5:* Fractional decrease in EE as function of WFE

over the period March 31 to Oct 3, 2024, as fitted in Figure 1. *Column #6*: Relative usage fraction of each filter as derived in Section 4.2.3.

4 Time breakdown of JWST Usage

A key quantity in equation (15) for the WFE threshold that should trigger a WFC is the fraction of the time ξ during which JWST is performing on-sky integrations of the kind that are well described by the adopted S/N equations. We discuss the many different considerations that affect this factor.

4.1 On-sky Science Time Fraction

JWST only spends a fraction η of the time collecting photons from on-sky science exposures. The remainder is spent on slews, guide-star acquisitions, instrument overheads, etc. The latter are "charged" to observers in an approximate or statistical sense based on observatory models. Therefore, every accepted JWST program has in its APT file a value for both its "Science Time" (the total time collecting photons from the sky) and a "Charged Time" (the total wall clock time that elapses to collect these photons, including all applicable overheads). The fraction η can be estimated as the sum of the Science Time for all observing programs, divided by the sum of their Charged Time.

We obtained a spreadsheet that lists all JWST programs through Cycle 4 known to the Proposal Planning System, with their respective values for the Science Time and Charged Time (T. Roman 2025, priv. comm.). Results from analysis of this spreadsheet are listed in Table 3. We selected all programs classified as either General Observer (GO), Guaranteed Time Observer (GTO), or Director's Discretionary (DD). We then subdivided these programs into the categories of Large (≥ 130 hours), Medium (50-130 hours), Small (20-50 hours), and Very Small (< 20 hours).¹⁰ The table lists the total number of programs in each category, as well as the fraction f of the total time that is made up by each category. The ratios of the summed Science Time and Charged Time values yield the listed estimates of the on-sky fraction η . To estimate the random uncertainty on each η value, we determined the values for each of Cycles 1, 2, 3, and 4 separately, and then determined the error in the mean over those cycles. Table 3 shows that the inferred value for η depends little on program size but tends to be slightly smaller for the Very Small programs. The bottom row of Table 3 lists the results when all programs are grouped together, independent of program size. This yields a final on-sky estimate $\eta = 60.4\% \pm 0.8\%$.¹¹

One source of systematic uncertainty in this result is that the concept of Charged Time is approximate, and does not capture the intricacies of all observatory overhead activities. Another source of systematic uncertainty is provided by calibration programs. These are included in the overhead quantified by the Charged Time and therefore are not counted here as on-sky observations. While many calibration programs are indeed "internal" (e.g., darks, lamps, etc.), many others do observe the external sky. However, those that do are not generally in the

¹⁰ These definitions have been slightly different in different Cycles. Here we use the definitions used for Cycle 4, independent of the cycle to which a program belongs.

¹¹ This result is similar to the $\sim 60\%$ fraction of the wall-clock time during which the FGS is guiding (e.g., Telfer et al. 2026, in prep.). This provides an independent sanity check on the result presented here.

background-limited regime and hence are not subject to the S/N arguments presented above. In this sense, it is indeed reasonable to not consider calibration programs as part of the on-sky time. Nonetheless, to capture the systematic uncertainties introduced by these arguments we adopt a final estimate $\eta = 60.4\% \pm 5.0\%$ in our subsequent analysis. Henceforth, this and other uncertainties are propagated in Monte-Carlo fashion.

Table 3: Breakdown of GO/GTO/DD science-time fraction by Program Category

Category	Proposals	f_{cat}	η
Large	29	0.159	0.630 ± 0.015
Medium	121	0.265	0.630 ± 0.010
Small	402	0.357	0.601 ± 0.017
Very Small	735	0.220	0.557 ± 0.013
TOTAL	1287	1.000	0.604 ± 0.008

Notes: *Column #1:* Program category. *Column #2:* Number of programs through JWST Cycle 4. *Column #3:* Corresponding fraction of the total hours. *Column #4:* Ratio of the total “Science Time” to total “Charged Time”.

Table 4: Cycle 4 breakdown by Instrument Mode

Category	f_{mode}	Comments
MIRI Coronagraphy	0.016	see Section 4.2.7
MIRI Imaging	0.049	see Section 4.2.7
MIRI LRS	0.105	see Section 4.2.7
MIRI MRS	0.177	see Section 4.2.7
NIRCam Coronagraphy	0.015	see Section 4.2.3
NIRCam Grism Time Series	0.007	see Section 4.2.1
NIRCam Imaging	0.140	see Section 4.2.3
NIRCam Time Series	0.006	see Section 4.2.1
NIRCam WFSS	0.020	see Section 4.2.4
NIRISS Imaging	0.000	see Section 4.2.5
NIRISS AMI	0.002	see Section 4.2.5
NIRISS SOSS	0.031	see Section 4.2.1
NIRISS WFSS	0.000	see Section 4.2.5
NIRSpec Bright Object Time Series	0.101	see Section 4.2.1
NIRSpec Fixed Slit Spectroscopy	0.035	see Section 4.2.6
NIRSpec IFU Spectroscopy	0.108	see Section 4.2.2
NIRSpec MOS	0.189	see Section 4.2.6
TOTAL	1.000	

Table 4. *Column #1:* Instrument Mode. *Column #2:* Fraction of allocated prime hours in JWST Cycle 4. *Column #3:* Reference to the section that discusses whether/how observations with the mode have their S/N affected by small changes in WFE. Modes highlighted in dark grey are unaffected for the sources typically observed with this mode, or have zero prime usage in Cycle

4. Modes highlighted in light grey are affected, but have their resolution affected in only one detector dimension. Modes shown without highlighting are affected and have their resolution affected in both detector dimensions.

4.2 Observing Mode Dependence

Table 4 provides a breakdown of all accepted Cycle 4 GO programs by instrument mode, based on data presented in Moro-Martin (2024). This is restricted to prime observations and excludes parallel observations. This is because exposure times are normally driven by the S/N of the prime observations, with the parallel observations playing only a secondary role. Observations with different modes are affected differently by WFE variations, as discussed below.

4.2.1. Bright-Object Modes

There are a number of science instrument modes that are primarily used for bright objects. This includes NIRCam grism time series, NIRCam time series, NIRISS SOSS, and NIRSpec bright object time series. For bright objects, the noise is generally dominated by the object, and not the background. A decrease in EE can then be compensated entirely by using a slightly larger aperture, without increasing the noise. Hence, while this degrades the spatial resolution, the S/N is unaffected. We therefore exclude all bright-object modes from further consideration. These comprise a fraction $\zeta_{\text{bright}} = 0.145$ of the Cycle 4 observing time.

4.2.2. Extended-Object Modes

There are a number of other modes that are primarily used for extended objects. This includes NIRSpec IFU spectroscopy, as well as MIRI MRS (which also uses an IFU). For an extended object, subtle variations in the PSF only minimally affect the object's light distribution. Moreover, the extraction aperture used is generally defined by the size of the object or the characteristics of the instrument (e.g., spaxel size), and not by the PSF characteristics. We therefore exclude all extended-object modes from further consideration. These comprise a fraction $\zeta_{\text{ext}} = 0.285$ of the Cycle 4 observing time.

4.2.3. NIRCam Imaging

NIRCam imaging can target various kinds of objects. This includes point sources that are observed in the background-limited regime, to which the formalism of Section 2 applies (e.g., white dwarfs in globular clusters). However, such observations make up only a fraction f_{app} of all NIRCam imaging observations. Sometimes the focus is instead on bright point sources that are not background limited (e.g., astrometry of high- S/N stars in nearby dwarf galaxies). And more importantly, often the focus is instead on extended sources (e.g., distant background galaxies, the science targets for which JWST was originally envisaged). For bright and extended targets, WFE degradation only minimally affects the S/N , as already discussed above, so we need to exclude such observations from our formalism. However, it is not straightforward to estimate what fraction of all NIRCam imaging observations falls in each category. Even within a single observing program, the science may depend on extended objects, as well as bright and faint point sources, altogether. So here we simply assume that our formalism applies to a fraction $f_{\text{app}} = 0.50 \pm 0.25$ of observations, with the generous error reflecting the ignorance. For the

present report, we treat coronagraphy similar to other imaging. Hence, we exclude a fraction $\zeta_{\text{NIRCam-im}} = (1 - f_{\text{app}}) \times (14.0 + 1.5)\%$ from further consideration.

For the remaining NIRCam imaging observations, we need to determine the average $\langle s_e \rangle$ for the different wide-band filters, weighted by the filter usage (see equation 16). To determine the latter, we obtained a table that lists the number of GO/GTO/DD observations in the Mikulski Archive for Space Telescopes (MAST) for each of the NIRCam filters (M. Boyer 2025, priv. comm.). Table 2 lists the implied relative usage fractions for the wide-band filters, normalized such that the filters in the NIRCam short-wave (SW) and long-wave (LW) channels each add up to 0.5. The reason for this normalization is that the SW and LW filters are used in parallel, so the total observation fraction for each channel must be the same.¹² The usage fractions for the wide filters in the 1-5 μm range are fairly similar, but the F070W and F090W filters are used significantly less often. This is probably because JWST was not designed and optimized for low-wavelength observations, and such observations can also often be accomplished (in part) by other telescopes. For our analysis we need the filter usage as fraction of the observing time, whereas Table 2 provides the usage as a fraction of the number of observations. This should be reasonable proxy, given that there is no obvious reason why exposures with some wide filters should be systematically longer than in other wide filters. However, that is certainly possible. To account for this, we assume that each of the usage fractions in Table 2 has an uncertainty equal to 25% of its value.

With this model, we can use the values of $\langle s_e \rangle$ for the different filters, derived from Figure 1 and listed in Table 2, to determine the weighted average as

$$\langle s_e \rangle_{\text{NIRCam}} = (2.02 \pm 0.18) \times 10^{-3} \text{ nm}^{-1} \quad . \quad (18)$$

If instead we calculate weighted averages separately for the filters in the SW and LW channels, then

$$\langle s_e \rangle_{\text{SW}} = (3.67 \pm 0.23) \times 10^{-3} \text{ nm}^{-1} \quad . \quad (19)$$

$$\langle s_e \rangle_{\text{LW}} = (3.66 \pm 0.23) \times 10^{-4} \text{ nm}^{-1} \quad . \quad (20)$$

We have focused here on the broad-band filters. However, the value of s_e depends primarily on the central wavelength, and only weakly on the bandwidth. Hence, the results should approximately apply also to the medium- and narrow-band filters, assuming their usage fractions depend on wavelength similarly as assumed in the adopted model. Moreover, the wide filters are used for 69% of all NIRCam imaging observations, so this assumption affects a minority of the observations.

The NIRCam LW and SW channels operate in parallel at any given time. Usually, the data from both channels are used in any science analysis. Comparison of equations (19) and (20) above

¹² In reality, the usage fractions of the wide SW filters are a factor 1.17 larger than what is listed in Table 2, while the fractions for the wide LW filters are a factor 0.83 smaller. This is because the medium and narrow filters in the LW channel (including e.g. the F335M PAH filter) are somewhat more popular than those in the SW channel.

implies that WFE variations affect the EE and S/N most in the SW channel. Hence, it is this channel that drives changes to the required exposure times. Hence, we adopt the value of $\langle s_e \rangle_{SW}$ for all NIRCcam imaging within the formalism of Section 2.

4.2.4. NIRCcam WFSS

S/N calculations for spectroscopy are generally more complex than for imaging, which is beyond the scope of the present report to explore in detail. However, a simple limit case is to assume that the spectrum of a source is a collection of delta-function emission lines. In this case, NIRCcam Wide Field Slitless Spectroscopy (WFSS) with one of its gratings produces a collection of separate sources on the detector. These will resemble point sources in the spatial direction, but the width in the wavelength direction will be determined primarily by the spectral resolution, and not the PSF. Hence, WFE variations will affect the source width in one, instead of two dimensions. This implies that to lowest order, the change in EE is the square-root of what it is for direct imaging. In the low-order Taylor regime of small variations, this implies that the value of $\langle s_e \rangle$ for direct imaging must be divided by 2. Since the NIRCcam WFSS mode covers the wavelength regime from 2.4 - 5.0 micron, we use the $\langle s_e \rangle$ imaging value for the LW channel.

As for the case of NIRCcam imaging, we assume that the formalism of Section 2 only applies to a fraction $f_{app} = 0.50 \pm 0.25$ of observations, mainly because the WFSS mode often targets extended objects (e.g., distant galaxies). Hence, we exclude a fraction $\zeta_{NIRCcam-ss} = (1 - f_{app}) \times 2.0\%$ from further consideration.

4.2.5. NIRISS

The Near-Infrared Imager and Slitless Spectrograph (NIRISS) plays only a limited role for the present report. Most of its use is for the single-object slitless spectroscopy (SOSS) mode, or for parallel observations, neither of which effect the present discussion. NIRISS imaging and WFSS were not used in prime mode in Cycle 4. But had they been, they could have been handled similarly to the corresponding NIRCcam modes. This leaves only 0.2% of Cycle 4 in Aperture Masking Interferometry (AMI). As for NIRCcam coronagraphy, we treat this similar to regular imaging. However, this mode covers the wavelength regime from 2.4 - 4.8 micron, so we use the value of $\langle s_e \rangle$ determined for the NIRCcam LW channel.

As for the case of NIRCcam imaging, we assume that the formalism of Section 2 only applies to a fraction $f_{app} = 0.50 \pm 0.25$ of observations, mainly because the AMI mode often targets both (faint) exoplanets and (extended) debris disks. Hence, we exclude a fraction $\zeta_{NIRISS} = (1 - f_{app}) \times 0.2\%$ from further consideration.

4.2.6. NIRSpec

NIRSpec has two observing modes, fixed-slit spectroscopy and multi-object spectroscopy (MOS), aside from the ones already excluded in Sections 4.2.1 and 4.2.2. We make the same simplifying assumptions as for NIRCcam WFSS in Section 4.2.4. Hence, the values of $\langle s_e \rangle$ for direct imaging are divided by 2. The NIRSpec spectral elements cover the same wavelength regime (~0.7-5 micron) as the NIRCcam wide-band filters. Hence, we use the $\langle s_e \rangle_{NIRCcam}$ average over all filters from equation (19).

As for the case of NIRCam imaging, we assume that the formalism of Section 2 only applies to a fraction $f_{\text{app}} = 0.50 \pm 0.25$ of observations, mainly because these NIRSpec modes often target extended objects (e.g., distant galaxies). Hence, we exclude a fraction $\zeta_{\text{NIRSpec}} = (1 - f_{\text{app}}) \times (3.5 + 18.9)\%$ from further consideration.

4.2.7. MIRI

The Mid Infrared Instrument (MIRI) provides various modes for observations at wavelengths above ~ 5 micron. Figure 1 and Table 2 show that at these wavelengths, any degradation of the EE due to the level of WFE variations considered here (≤ 10 nm) is negligible. Hence, the S/N of such observations is not meaningfully affected. We therefore exclude all MIRI modes from further consideration. These comprise a fraction $\zeta_{\text{MIRI}} = 0.170$ of the Cycle 4 observing time (not counting the MIRI/MRS time already excluded in Section 4.2.2.).

4.3 Combined Results

We now have all the components needed to estimate the fraction of the time during which JWST is performing on-sky integrations of the kind that are well described by the adopted S/N equations. The fraction of wall-clock time for which the S/N is affected by WFE degradation is

$$\begin{aligned} \xi &= \eta \left(1 - \zeta_{\text{bright}} - \zeta_{\text{ext}} - \zeta_{\text{NIRCam-im}} - \zeta_{\text{NIRCam-ss}} - \zeta_{\text{NIRISS}} - \zeta_{\text{NIRSpec}} \right) \\ &= (0.604 \pm 0.050) (1 - 0.631 \pm 0.100) = 0.223 \pm 0.063 \quad . \end{aligned} \quad (21)$$

The weighted average $\langle s_e \rangle$ over all the modes that do contribute to the affected fraction is

$$\begin{aligned} \langle s_e \rangle &= \{ [(0.140 + 0.015)\langle s_e \rangle_{\text{SW}}] + [((0.020/2) + 0.002)\langle s_e \rangle_{\text{LW}}] + [((0.035 + 0.189)/2)\langle s_e \rangle_{\text{NIRCam}}] \\ &\quad \} / (0.140 + 0.015 + 0.020 + 0.002 + 0.035 + 0.189) \\ &= (1.99 \pm 0.12) \times 10^{-3} \text{ nm}^{-1} \quad . \end{aligned} \quad (22)$$

Note that the factor f_{app} enters into equation (21) through several of the ζ values, but it drops out of equation (22) because it scales all modes in the nominator and denominator equally.

The extra time required to add a WFC activity is $\Delta T_c = 47$ minutes, based on the values given in OTE Memo #5. That report also implies that the OTE WFE drifts at a rate $s_w = 0.0862 \pm 0.0513$ nm/day, based on measurements in recent years. We now have estimates of all the quantities that enter into equation (15). Substitution yields that the WFE error threshold that should trigger a WFC equals

$$\Delta \text{WFE} = 1.80 \pm 0.54 \text{ nm}. \quad (23)$$

The average cadence between WFC activities (i.e., $\Delta \text{WFE}/s_w$) is then

$$\Delta T_{\text{WFC}} = 23.4 \pm 7.5 \text{ days} \quad . \quad (24)$$

This is close to (and statistically consistent with) a roughly monthly cadence.¹³

Another quantity of interest is the integrated WFE increase ΔIW relative to the baseline, i.e., the area under the trend of ΔWFE vs. time. Assuming as before a linear slope s_w for this curve, ΔIW increases quadratically with the time T_{\max} over which the WFE evolves as

$$\Delta IW = (1/2) s_w T_{\max}^2 . \quad (25)$$

Using equations (9) and (11) this can also be written as

$$\Delta IW = \Delta T^- / (2\xi s_e) . \quad (26)$$

Hence, ΔIW is linearly proportional to the added time ΔT^- that must be spent to reach the same S/N for a representative sequence of observations, in the absence of a WFC. Substitution of ΔT_{WFC} from equation (24) for T_{\max} in equation (25) implies that the optimal value at which to trigger a control is

$$\Delta IW_{\text{opt}} = 20.5 \pm 9.2 \text{ nm day} . \quad (26)$$

5 Interpretation and Conclusions

In practice, JWST is not operated in a manner that guarantees each program a specific S/N . Instead, each program is awarded a specific number of hours. Observations are executed during these hours, independent of JWST image quality at the time of the observations. Observers estimate their time requests, given the S/N required for their science, using the Exposure Time Calculator (ETC). The ETC makes conservative assumptions about image quality, so that reasonable variations in image quality do not jeopardize the ability to achieve the science goals. Hence, changing the WFE threshold from the current value would not actually save any time, and we should look at our calculations differently. The WFE threshold derived here does not merely minimize observing time at fixed S/N , but as a direct corollary, it also maximizes the S/N at fixed observing time. The latter view corresponds to how JWST is actually operated. Hence, the threshold in equations (23), (24) and (26) is the value that optimizes the S/N of the grand-total JWST observing program.

¹³ Readers may find it useful to have a simple approximate understanding of the order of magnitude of this result. To this end, note the following. The value of s_w corresponds to an increase of 8nm in ~ 3 months. The s_e values in Table 2 show that at a typical wavelength of 2 μm , an 8 nm increase in WFE yields $\sim 1\%$ decrease in EE. The average decrease over the 3 month period to reach 8nm is half that. But equation (6) shows that the exposure time scales as EE^{-2} , which in first-order Taylor approximation yields multiplication by a factor 2. So on average, the added exposure time to reach the same S/N is ~ 1 day ($\sim 1\%$ of ~ 3 months). Equation (21) shows that this applies to only $\sim 1/5$ th of the wall clock time, so that reduces the estimate to ~ 5 hr. That is 5 times longer than the extra ~ 1 hr it takes to do a WFC. So it is more efficient to do a WFC sooner than 3 months, rather than to keep exposing that long. The break-even point is reached at $\sim 3/5$ months, which is ~ 18 days. This is close to (and statistically consistent with) the more detailed answer in equation (24).

The inferred ΔWFE threshold is well below the value of 8 nm in current operational use. Hence, we could (very slightly) increase the overall S/N of the JWST observing program by performing WFC more frequently. This would have the added benefit of yielding on average better image quality, although at levels of several nm this may be noticeable only in highly specialized applications (e.g., coronagraphy). Either way, this is valuable in its own right, aside from S/N considerations.

Despite the benefit of an overall increases in S/N that can be achieved with more frequent WFC, it does increase the amount of operational overhead spent on WFS&C activities. Such increases are undesirable. However, this can be avoided by trading time spent on WFS with time spent on WFC. OTE Memo #5 showed that the current WFS cadence of 4 days is actually non-optimal, and too frequent. The total time spent on WFS&C activities each year is given by equation (1) of that document. To lowest order, if the time ΔT_{WFC} between WFC activities is decreased by a factor γ , then the total total time spent on all WFS&C activities remains the same if the WFS cadence is increased by a factor

$$(1 - [(D_c/D_s) - 1][x/\Delta T_{WFC}][(1/\gamma) - 1])^{-1} . \quad (25)$$

Here x is the WFS cadence, which is currently 4 days. So if this cadence is increased to 4.5 days, then the amount of time saved would equal the added time spent to perform WFC at the WFE threshold given by equation (23). This new WFS cadence would still be below the optimal value of 5.98 ± 0.95 days derived in OTE Memo #5.

In a nutshell, the question that was addressed in this report is the following: if an extra ~ 1 hour were to be available, would the S/N of approved JWST observing programs be better off by: (a) proportionally increasing their exposure times? or (b) executing an extra WFC activity? Given how we currently operate the telescope, we found that the answer is (b). But of course, those are not the only options. One could alternatively consider: (c) approve another very small observing program to obtain new and different science exposures for ~ 1 hour. Whether this is better than very slightly increasing the S/N of the already approved programs is not an engineering trade, but a science policy/merit question that is beyond the scope of this report.

Aside from this more philosophical point, the combined upshot from OTE Memo #5 and the present report is that the current operational settings for when to perform WFS and WFC can be further optimized. WFS is performed slightly too frequently, while WFC is performed too rarely. By increasing the WFC cadence while somewhat decreasing the WFS cadence, the S/N of the grand-total JWST program can be (very slightly) improved without increasing the total time spent on WFS&C activities.

The preceding does *not* imply that the operational criteria for when to initiate a WFC activity should be modified to exactly reflect either of equations (23), (24) or (26). For example, random fluctuations in WFS measurements (typically less than 1 nm RMS relative to the linear trends given by equation (1); e.g. OTE Memo #5), which have not been explicitly considered here, may limit how frequently it is practical to execute WFCs. Moreover, WFC has associated cost in the

labor that needs to be invested to create, upload, execute, and verify the required WFC commands.

Similarly, increasing the WFS cadence would also have some potential downsides, as discussed in Section 7 of OTE Memo #5. Hence, the goal should be to move the criteria in the direction of more frequent WFCs, but exactly by how much should be a broader discussion that incorporates additional operational considerations.

Note also that there are various ways in which the operational criteria for triggering a WFC could be updated so as to achieve more frequent controls. For example, the ΔWFE threshold could be lowered from 8 nm to a value closer to equation (23). Alternatively, this criterion could be left as is, but a new criterion could be added to limit either the elapsed time or the integrated ΔIW since the preceding WFC (see equations (24) and (26), respectively). The latter would make more sense, since it actually depends on the specific WFE evolution since that control. Also, because it is an integrated quantity, it is less sensitive to noise than ΔWFE itself. Equation (26) implies that a threshold criterion on ΔIW would be equivalent to setting a limit on the added time that would be needed to reach the same S/N for a representative sequence of observations. Such a limit on “added time” directly connects to the key argument of the present report.

6 Acknowledgements

I am grateful: to Matt Lallo and the members of the WFS&C team for suggesting the exploration of the problem addressed in this report; to Marcio Melendez for creating an [STPSF jupyter notebook](#) in the [JWST Data Analysis Tools Repository](#) that served as a useful starting point for the calculations in Section 3; to Marshall Perrin, Nicolas Flagey and Randal Telfer for suggesting and exploring the ΔIW integrated WFE metric; and to Tony Roman and Martha Boyer for kindly researching and making available the JWST Program and NIRCcam usage statistics analyzed in Sections 4.1 and 4.2.3, respectively.

7 Bibliography

Gardner, J. P., Mather, J. C., Abbott, R. 2023, [PASP, Vol. 135, Iss. 1048, id. 068001](#)

Flagey, N., Beck, T., Lallo, M., et al. 2025, JWST Technical Report JWST-STScI-009205 (under review), OTE Science Performance Memo 6: JWST Wavefront Sensing and Control Operations and Efficiencies

Lajoie, C.-P., Lallo, M., Melendez, M., Flagey, N., 2023, JWST Technical Memorandum JWST-STScI-008497, [OTE Science Performance Memo 2: A Year of Wavefront Sensing with JWST in Flight: Cycle 1 Telescope Monitoring & Maintenance Summary](#)

McElwain, M. W., Feinberg, L., Perrin, M., et al. 2023, [PASP, Vol. 135, Iss. 1047, id. 058001](#)

Moro-Martin, A. 2025, [JWST Cycle 4 Peer Review Results, presented to the JSTUC, Feb 28, 2025](#)

Savino, A., Gennaro, M., Dolphin, A. E., et al. 2024, [ApJ, 970, 36](#)

Telfer, R., et al. 2026, JWST Technical Memorandum, in prep.

van der Marel, R. P., 2025, JWST Technical Memorandum JWST-STScI-009059, [OTE Science Performance Memo 5: The Optimal Wavefront Sensing Cadence](#) (OTE Memo #5)